American Mineralogist, Volume 84, pages 112–119, 1999

Dehydration dynamics of analcime by in situ synchrotron powder diffraction

GIUSEPPE CRUCIANI[1,*] AND ALESSANDRO GUALTIERI[2]

[1]Istituto di Mineralogia, Università di Ferrara, Ferrara, Italy
[2]Dipartimento di Scienze della Terra, Università di Modena, Modena, Italy

ABSTRACT

The continuous structural transformation of tetragonal analcime ($Na_{15.87}Al_{15.20}Si_{32.64}O_{96}\cdot 16.3H_2O$) upon dehydration was studied, using Rietveld structure analysis of temperature-resolved powder diffraction data collected using synchrotron radiation. The variation of the *a*-*c* axis length difference and normalized intensity of the (200) reflection as a function of temperature suggest that tetragonal analcime evolves toward a cubic structure at high temperature. The removal of water was accompanied by a spreading of the initial Na sites into many positions bonded to the framework O atoms. The migration of H_2O molecules through the [111] channels during dehydration caused the six-member ring apertures to open as widely as possible: this was accompanied by a twisting of the tetragonal prism, constituting the analcime framework, which led to an opposite tilting of tetrahedra connecting the prisms. These modifications induced by water diffusion are not energetically favored because they would increase the elastic energy of the system, and require a substantial thermal activation energy. The analcime framework reached a maximum distortion at about 650 K, the temperature of complete water loss, then underwent a relaxation process during which the T-O-T angles were restored to the starting value. The relative variation of cell volume associated with the opening of wide six-member ring channels during water migration, and then due to the framework relaxation process after complete dehydration, provides an explanation of the ''negative thermal expansion'' (i.e., volume contraction) effect in dehydrated analcime, which is complementary to that based on the Rigid Unit Modes theory.

INTRODUCTION

Analcime is a zeolite (and feldspathoid) having a complex aluminosilicate framework that is common to all leucite-type feldspathoids (Merlino 1984). The maximum topological symmetry of analcime is cubic, *Ia*3*d* (Taylor 1930; Calleri and Ferraris 1964; Knowles et al. 1965; Ferraris et al. 1972). However, deviations from cubic symmetry are well known (Mazzi and Galli 1978; Hazen and Finger 1979). Regarding the genetic conditions, analcimes have been divided into five groups (Luhar and Kyser 1989): primary igneous analcimes (called P-type); those formed by cation exchange from leucite (L-type or X-type); hydrothermal analcimes (H-type); sedimentary analcimes (S-type); and metamorphic analcimes (M-type). X-type analcimes are typically cubic, whereas H-type analcimes have tetragonal, rhombohedral, or orthorhombic symmetry (Kapusta and Wlodyka 1997).

Dehydration of analcime is a one step process, as evidenced by the DTA and TG curves that show only one maximum at roughly 620 K; this corresponds to the loss of H_2O molecules in the sole symmetry-independent site in the cubic structure (Gottardi and Galli 1985). Kim and Burley (1971; 1980) suggested that a structural phase transition occurs upon dehydration, which leads to a stable high-temperature dehydrated phase (high-analcime) with a unit-cell volume smaller than that of low-analcime. The kinetics of the dehydration process in *H*-type (hydrothermal) and X-type (cation exchange from leucite) cubic analcimes studied by DTA methods show apparent activation energies for the H-type analcimes that are four times greater than for X-type analcimes (Giampaolo and Lombardi 1994; Line et al. 1995). Cubic analcime has recently been the subject of a series of papers, given its similarity to the structure of leucite that has displacive phase transitions currently of great interest (Palmer et al. 1996). Putnis et al. (1993) reported that cubic analcime transformed to tetragonal upon heating at a temperature of about 600 K, depending on the atmosphere, mainly due to the *c* axis contraction. After dehydration, the unit cell became cubic again, due to the increase of the *c* axis, and it remained cubic until analcime turned to amorphous. Line (1995) found no displacive phase transition associated to the high-temperature dehydration process of cubic analcime. Line et al. (1996) also studied the low-temperature behavior of analcime by high-resolution neutron powder diffraction in the range 30–300 K, and found no sign of any phase transition.

The present investigation strives to (1) give a more

* E-mail: cru@dns.unife.it

0003–004X/99/0102–0112$05.00

exhaustive picture of the analcime dehydration, and to ascertain whether any phase transition occurs before the collapse of the structure at high temperature; (2) give a detailed picture of the sodium migrations, if any, during the dehydration process, and of their relationship to water removal; and (3) follow the overall process in a tetragonal natural analcime and compare the data to the process in cubic analcime (Putnis et al. 1993; Line 1995; Line et al. 1996).

Data collection and Rietveld refinement

The sample from Val di Fassa, Trento (Italy) is classified as ''ANA 2 (28)'' in the collection of the Mineralogy Museum at the University of Modena. A sample from the same locality was studied and labeled ''ANA 2'' by Mazzi and Galli (1978) in their single crystal study.

The temperature-resolved powder diffraction data were measured on beam-line X7B at the National Synchrotron Light Source (NSLS), Brookhaven National Laboratory (U.S.A.). The optics of the beam-line are described by Hastings et al. (1983). Temperature-resolved experiments were performed by continuous in-situ heating of an analcime sample packed in a 0.7 mm capillary, with a measured packing coefficient of 0.48, open to air on one side. The heating rate was 4.2 K/min. The two-dimensional diffraction patterns were recorded on the 3 mm slit-delimited portion of a translating flat imaging plate (Norby 1997), which had a translation rate with respect to the temperature increase of 2.5 pixels/K. External standard LaB_6 was used to calibrate the wavelength (λ = 0.9602 Å), as well as to determine the zero-shift position, sample to detector distance, and tilting angle of the image plate detector. These experiments allowed the collection of powder patterns, with a maximum $\sin\theta/\lambda$ of 0.45, suitable for Rietveld refinement. Powder patterns were extracted from the collected image using a specially developed program that performs a line integration procedure. To obtain 35 powder patterns in the range 363–1064 K, a 25 pixel width (i.e., over 10 K) of the integration line was chosen, and the extraction procedure was carried out in steps of 50 pixels (i.e., every 20 K). This temperature step was selected after several tests and found to be consistent with the kinetic rate of the analcime transformation. From the above parameters, a variance in the temperature scale of ± 5 K could be calculated. Unfortunately, the re-crystallization and consequent deformation of the quartz-glass capillary at $T > 1000$ K (cf. Fig. 1) imposed an upper temperature limit to the experiment. A powder pattern at 298 K [which was room temperature (RT)] was also collected.

Rietveld refinements were performed on each powder pattern using the GSAS program package (Larson and Von Dreele 1997). The presence of ($h00$: $h = 4n + 2$) type reflections (e.g., 200) on powder pattern of our analcime at RT (cf. Fig. 1) confirmed Mazzi and Galli's (1978) report of deviation from the cubic $Ia3d$ symmetry. The refinement of the first pattern collected at 363 K was started using their structural model of tetragonal Val di Fassa analcime with space group $I4_1/acd$. Trials using the cubic (Ferraris et al. 1972) and orthorhombic (Mazzi and Galli 1978) models yielded less satisfactory results in terms of profile fitting. The diffraction peaks were modeled with a pseudo-Voigt function with three Gaussian and two Lorentzian line-broadening terms. The background curve was fitted with a Chebyshev polynomial with 24 coefficients. As a time-saving procedure, only fixed points were used in the early stages of the refinement for modeling the background function. The refinement details for patterns at T = 298 K, T = 632 K, and T = 921 K are given in Table 1. The refined atomic coordinates, thermal parameters, and occupancy fractions for selected data sets are reported in Table 2. Selected interatomic distances and angles are given in Table 3. The complete set of structural parameters refined at all temperatures is given in Table 4[1]. The observed and calculated patterns for all diffractograms are available on request from the authors.

An electron microprobe analysis was carried out using an ARL-SEMQ instrument operating at 15 kV and 20 nA. The electron beam was defocused to about 20 μm. Online data reduction was based on the PROBE program (Donovan 1995). The thermogravimetric analysis was performed with a TG/DTA SEIKO SSC 5200 instrument using a heating rate of 4 K/min, approximately equal to the one employed for the diffraction experiment in air. The unit-cell composition determined for our analcime sample is $Na_{15.87}Al_{15.20}Si_{32.64}O_{96}\cdot 16.3H_2O$; it is similar to what reported by Mazzi and Galli (1978) for their ''ANA 2'' sample.

Results and discussion

Room-temperature crystal structure

The analcime framework is made up of singly connected four-member ring chains wrapped around square prisms. Three interconnected prismatic cages constitute one large, highly distorted cage which is delimited by four-, six-, and eight-member tetrahedral rings. The center of the large cage (W site) is occupied by one water molecule bonded to Na cations—located at the center of each prismatic cage (S sites)—which are each coordinated by two H_2O molecules and four framework O atoms. The mobility of ions and H_2O molecules within the irregular channel system is limited by the 1.6 × 4.2 Å free diameter of the eight-member ring along the [110] direction, and by the presence of the six-member rings axially arranged along [111]. In leucite, the water molecule in the W site is replaced by K atoms. According to Mazzi and Galli (1978), lowering of the symmetry in tetragonal analcime is caused by ordering of Al in the T1 site that, in turn, leads to a non-equivalent distribution of Na atoms

[1] For a copy of Table 4, Document AM-99-003, contact the Business Office of the Mineralogical Society of America (see inside front cover of recent issue) for price information. Deposit items may also be available on the American Mineralogist web site (see inside back cover of a current for web address).

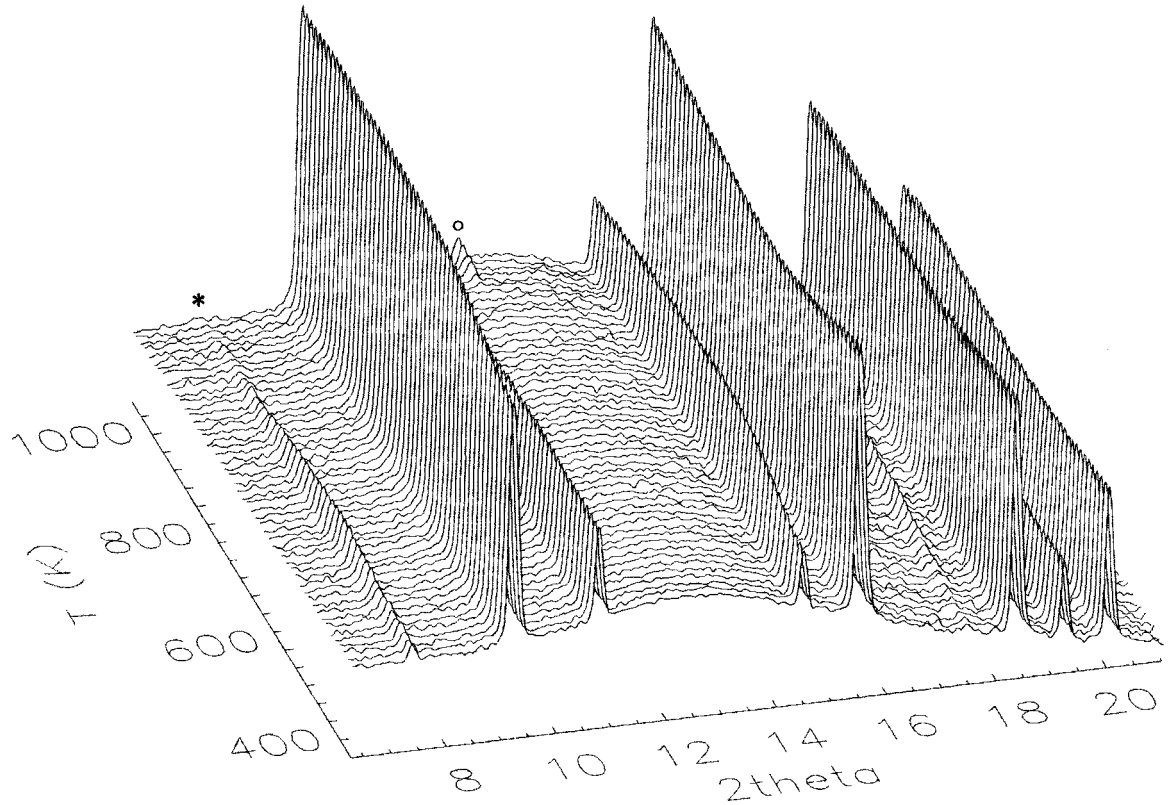

FIGURE 1. 3-D plot (2θ-intensity-temperature) for the dehydration process of analcime. The asterisk marks location of the (200) reflection, which is systematically absent in space group *Ia*3*d*. The circle indicates the (113) quartz peak from capillary re-crystallization for $T > 1000$ K.

over two symmetrically independent sites (Na1 and Na2). The results of our RT refinement are similar to those reported by Mazzi and Galli (1978) for their ''ANA 2'' sample. The mean T-O bond distances are consistent with a preferential partitioning of Al in the T1 site with respect to the T2, as observed by Mazzi and Galli (1978). The occupancy refinement of Na sites indicates an overall Na content of 15.76 atoms per unit cell, which is in good agreement with the chemical analysis and only slightly greater then that found by Mazzi and Galli (1978). Almost 90% of the whole Na content is located in the Na1 site.

TABLE 1. Experimental and refinement data for analcime from Val di Fassa, Italy

Temperature (K)	298	632	921
a (Å)	13.7295(3)	13.6717(2)	13.6251(2)
c (Å)	13.7036(4)	13.5997(5)	13.5870(4)
Cell volume (Å^3)	2583.1(1)	2542.0(1)	2522.3(1)
R_p (%)	3.72	4.13	2.83
R_{wp} (%)	5.20	6.16	3.97
R_{F^2} (%)	5.69	8.27	5.69
χ^2	3.0	5.5	2.1
No. of variables	45	52	51
No. of observations	4832	5057	5057
No. of reflections	311	360	346

Notes: Composition = $Na_{15.87}Al_{15.20}Si_{32.64}O_{96}\cdot 16.3H_2O$; Radiation = synchrotron X-rays; wavelength = 0.9602 Å; Diffraction geometry = Debye-Scherrer. $R_p = \Sigma[Y_{io} - Y_{ic}]/\Sigma Y_{io}$; $R_{wp} = [\Sigma w_i(Y_{io} - Y_{ic})^2/\Sigma w_i Y_{io}^2]^{0.5}$; $R_{F^2} = \Sigma|F_o^2 - F_c^2|/\Sigma|F_o^2|$; $\chi^2 = \Sigma w_i(Y_{io} - Y_{ic})^2/(N_{obs} - N_{var})$. Estimated standard deviations in parentheses refer to the last digit.

Many similarities exist between the room-temperature structures of tetragonal analcime and the Cs-substituted tetragonal leucite studied by Palmer et al. (1997). In both cases, the difference between *a*- and *c*-axis lengths is small if compared to K-leucite. The unit-cell parameters (a = 13.729 Å; c = 13.704 Å) refined for analcime at 298 K are similar to those reported by Palmer et al. (1997) for Cs-leucite at 298 K (a = 13.652 Å; c = 13.722 Å). The same similarity between analcime and Cs-leucite applies to the average distance between the water molecule in the W site and the six nearest O atoms (<W-O> = 3.377 Å in analcime; <W-O> = 3.350 Å in Cs-leucite); this distance is significantly shorter in K-leucite (<W-O> = 3.012 Å). Furthermore, as a comparison of the degree of framework distortion, in both Cs-leucite and analcime at RT the [111] structural channels are fully inflated, and the mean T-O-T angle is wider (144.0° for Cs-leucite; 143.5° in analcime) than in K-leucite (137.8°). Therefore, the structural model for Cs-leucite at room and high temperatures is a useful basis for understanding the temperature-dependent behavior of analcime.

TABLE 2. Positional and thermal parameters for analcime at 298 K, 632 K, and 921 K.

Atom	Type*	*x*	*y*	*z*	U_{iso}	Occupancy
			***T* = 298 K**			
T1	32g	0.1243(4)	0.1609(4)	0.4141(3)	0.038(1)	1.0
T2	16f	0.1619(3)	0.4119	⅛	0.039(2)	1.0
O1	32g	0.0990(5)	0.3734(4)	0.2188(4)	0.024(2)	1.0
O2	32g	0.2219(4)	0.1120(6)	0.3627(6)	0.055(3)	1.0
O3	32g	0.3582(6)	0.2179(4)	0.1052(6)	0.038(2)	1.0
Na1	16e	0.1343(8)	0	¼	0.083(3)	0.86(1)
Na2	8b	0	¼	⅛	0.083(2)	0.25(1)
W	16f	0.1165(10)	0.1335	⅛	0.069(3)	1.00
			***T* = 632 K**			
T1	32g	0.1235(5)	0.1592(3)	0.4134(3)	0.058(1)	1.0
T2	16f	0.1657(4)	0.4157	⅛	0.060(2)	1.0
O1	32g	0.1036(6)	0.3773(6)	0.2197(4)	0.059(3)	1.0
O2	32g	0.2183(5)	0.1065(6)	0.3558(6)	0.068(3)	1.0
O3	32g	0.3612(7)	0.2214(5)	0.1041(7)	0.079(3)	1.0
Na11	32g	0.1167(15)	0.0197(15)	0.2249(14)	0.079(3)	0.35(1)
Na12	32g	0.184(7)	0.182(6)	0.057(6)	0.079(3)	0.06(1)
Na21	32g	0.060(10)	0.217(9)	0.025(7)	0.079(3)	0.04(1)
W	16f	0.085(6)	0.1647	⅛	0.066(3)	0.11(2)
			***T* = 921 K**			
T1	32g	0.1222(4)	0.1638(3)	0.4133(3)	0.070(1)	1.0
T2	16f	0.1595(3)	0.4095	⅛	0.047(1)	1.0
O1	32g	0.0984(4)	0.3741(4)	0.2194(3)	0.066(2)	1.0
O2	32g	0.2225(3)	0.1122(5)	0.3662(5)	0.085(3)	1.0
O3	32g	0.3491(5)	0.2210(4)	0.1100(7)	0.106(3)	1.0
Na11	32g	0.2228(15)	0.1055(16)	0.0301(16)	0.104(4)	0.23(2)
Na12	32g	0.1698(14)	0.1736(16)	0.0696(16)	0.104(4)	0.16(1)
Na2	8b	0	¼	⅛	0.104(3)	0.10(1)
Na3	32g	−0.005(4)	0.070(5)	0.100(6)	0.104(3)	0.05(4)

Notes: Space group = $I4_1/acd$, origin at $\bar{1}$ (at 0, −¼, ⅛ from $\bar{4}$), as in Mazzi and Galli (1987), to allow comparison with *Ia*3*d* setting in cubic analcime. Estimated standard deviations in parentheses refer to the last digit.

* Number of positions and Wyckoff notation.

Temperature-dependent variation of cell parameters

The progressive cell-volume contraction on increasing temperature (Fig. 2) very closely resembles the typical TG weight loss of analcime. The main reduction occurs between 400 K and 650 K (−1.6%), and the final volume contraction at 921 K is about 2.4%. The slight lengthening of the *a* axis (Fig. 2) that occurs below 400 K can possibly be explained as a coupled effect of the *c* axis shortening, or it may be associated to the extraframework ion rearrangement during the initial water loss. The considerable contraction of both *a* and *c* cell parameters between 400 K and 650 K is clearly related to the main water loss of the system. The linear approach of *a* toward *c* at temperatures above 650 K might be interpreted as a tendency of the tetragonal analcime to undergo a transformation to a cubic structure. Such a phase transition would occur at a temperature exceeding the upper limit of our experiment. Our present data clearly show that a close relationship exists between the temperature and both the *a*-*c* axis length difference and normalized intensity of the 200 reflection (Fig. 3). Both these parameters might be regarded as indicators for the deviation from the cubic symmetry of the analcime framework. It appears that the temperature increase up to the complete loss of water enhances tetragonal splitting. After removal of water, however, the structure seems to evolve toward a cubic symmetry. This would be consistent with disappearance of the 200 peak at about 1070 K, due to systematic extinction in the *Ia*3*d* space group. If we assume a linear extrapolation of this trend to higher temperatures, the *a*-*c* difference would indicate that the cubic symmetry of the cell could only be reached far outside the stability field of analcime ($T > 1170$ K). However, Putnis et al. (1993) observed that a transition from tetragonal to cubic analcime actually occurred after dehydration.

Crystal-structure modifications upon dehydration

The occupancy refinement of the water site shows that the water loss is very large up to 650 K and is completed at about 720 K; this is consistent with the TG curve measured using the same heating rate (Fig. 4).

The water diffusion is accompanied by a simultaneous rearrangement of the Na atoms in the Na1 and Na2 sites (Fig. 5). The distribution of water and Na sites at different temperatures is depicted with respect to the nearest framework atoms, as projected along [110] showing the eight-membered ring (Fig. 6), and as viewed through the six-member ring window of the [111] channels (Fig. 7). The occupancy of the Na2 site is the most affected by the initial water removal (Fig. 5b). The complete diffusion of Na2 into a new Na21 split site (cf. Figs. 6b and 7b) reaches a maximum at about 530 K, and is then completely vacated at about 630 K. The rather large population of this new site at 530 K, together with some dis-

TABLE 3. Selected interatomic distances (Å) and angles (°) for framework and extraframework atoms

	298 K	632 K	921 K
T1-O1	1.610(5)	1.600(5)	1.602(5)
T1-O2	1.656(5)	1.678(7)	1.664(6)
T1-O3	1.667(6)	1.662(8)	1.707(7)
T1-O3′	1.702(5)	1.663(6)	1.647(6)
Mean	1.659	1.651	1.655
T2-O1 ×2	1.636(4)	1.630(6)	1.604(4)
T2-O2 ×2	1.638(4)	1.635(5)	1.639(4)
Mean	1.637	1.632	1.622
T1′-O1-T2	145.5(6)	148.5(6)	148.7(5)
T1-O2-T2	145.6(6)	139.0(6)	148.6(5)
T1-O3-T1′	139.2(7)	141.8(9)	131.9(6)
Mean	143.5	143.1	143.1
Na1-O2 ×2	2.489(8)		
Na1-O3′ ×2	2.501(9)		
Na1-W ×2	2.520(9)		
Na11-O2		2.55(2)	2.47(3)
Na11-O2′		2.47(2)	2.53(3)
Na11-O3		2.47(2)	2.57(3)
Na11-O3′		2.41(3)	2.66(2)
Na11-W		2.44(8)	
Na12-O1		2.50(9)	2.52(2)
Na12-O2		3.08(9)	
Na12-O3		2.55(1)	2.59(2)
Na12-O3′		2.342(8)	2.54(2)
Na2-O1 ×4	2.524		2.510(5)
Na2-W ×2	2.262		
Na21-O1		2.07(1)	
Na21-O1′		2.74(1)	
Na21-O3		2.05(1)	
Na21-O3′		3.00(1)	
Na21-W		2.89(1)	
Na3-O1			2.19(6)
Na3-O1′			2.18(8)
Na3-O2			2.25(5)
Na3-O3			2.41(8)

Note: Only distances within the 2.00–3.00 Å range are reported for extraframework positions. Estimated standard deviations in parentheses refer to the last digit.

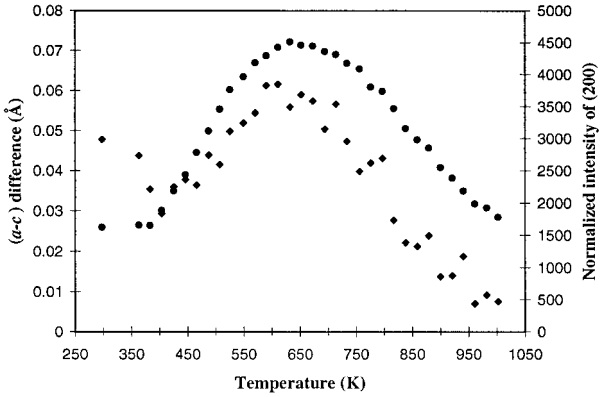

FIGURE 3. Plot of the *a*-*c* axis length difference (circles; left axis) and of the intensity of the (200) reflection, normalized against the refined scale factor (diamonds; right axis) vs. temperature ($T \pm 5$ K).

tances close to 2.5 Å from the Na1 sites, suggest that also H_2O molecules are statistically distributed in this position. At about 630 K the Na1 site splits also into a statistically occupied site (Na11), and a new related site (Na12) appears (see Figs. 6c and 7c). At this temperature, only about two H_2O molecules per unit cell out of the initial 16 are left in the system (cf. Fig. 4), whereas a content of almost 14 Na atoms per unit cell can be estimated from refined site occupancies (cf. Fig. 5a). It is likely that the remaining Na content is disordered within the zeolite cages. From 630 K to 950 K a gradual diffusion of Na atoms out of the Na11 site occurs, partially balanced by the increasing population of the Na12; the Na content from refined site occupancies decreases to about 10 atoms per unit cell. As expected, the complete removal of water leads to an increased interaction of Na atoms with the framework O atoms (cf. Figs. 6d, 6e, 7d, and 7e). At

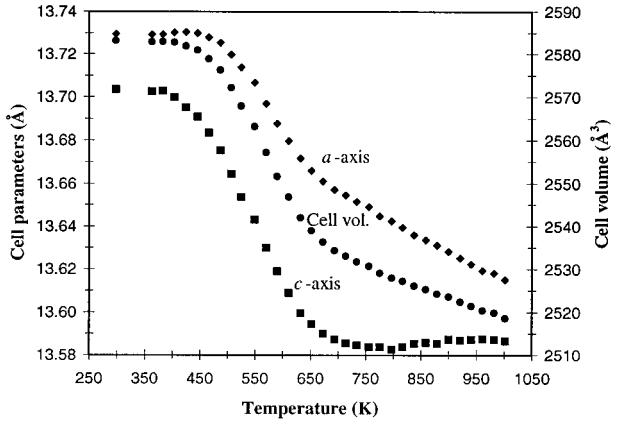

FIGURE 2. Plot of the *a* (diamonds) and *c* (boxes) cell axis lengths (left axis) and unit-cell volume (circles; right axis) vs. temperature. Estimated standard deviations on lengths and on volume less than 0.001 Å and 1 Å³, respectively. Variance in temperature equal to ±5 K.

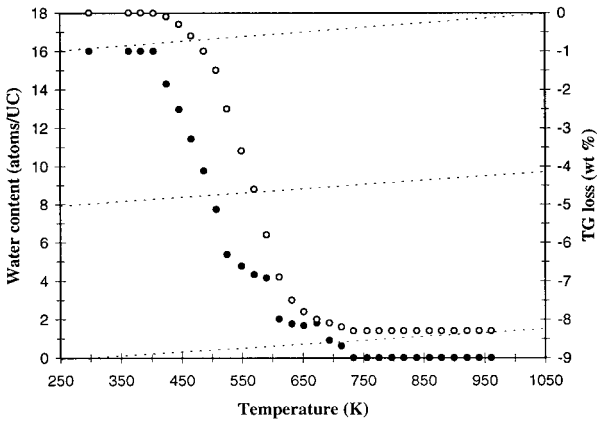

FIGURE 4. Comparison of the water content variation with temperature ($T \pm 5$ K) as calculated from the refined occupancy (solid symbols; left axis), and as measured by the TG loss (open symbols; right axis) on a sample from the same hand-specimen as that used for X-ray diffraction. Dotted lines connect corresponding values of water content.

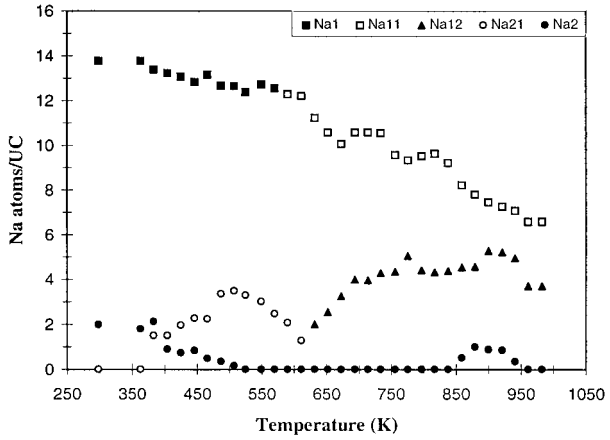

FIGURE 5. Variation of Na content from the refined occupancy for the extraframework Na1 and Na2 related sites (see legend for symbols), as a function of temperature ($T \pm 5$ K).

about 920 K the initial Na2 position seems to be populated again for a narrow temperature range and a small Na fraction occupies a new site (Na3).

The continuous structural distortions of the analcime framework associated with the dehydration process are well recorded by the changes of the T-O-T angles and the tilting of T2 about [1$\bar{1}$0] (Fig. 8). Although no sharp discontinuity is observed, a remarkable deformation of T1-O2-T2 and T1-O3-T1′ occurs in conjunction with the main water loss ($T \approx 650$ K) whereas the average T-O-T angle remains nearly constant (<T-O-T> $\approx 144°$). This behavior may be explained by the formation of more regular apertures, provoked by the passage of H_2O molecules through the six-member rings during dehydration. The corresponding variation undergone by the T-O-T angles can be regarded as a geometrical out-of-equilibrium state. After all the water has been released, the out-of-equilibrium T-O-T angles are brought back close to the original values. Similarly, Line (1995) found that in cubic analcime the six-membered ring appears to stay open until all the water has gone.

In accord with the model devised for leucite by Palmer et al. (1997), the temperature-dependent distortion mechanism in analcime can be described as a twisting of tetragonal prisms in which the upper four-membered ring rotates relative to the lower ring about the [001] axis. Temperature reduction or decrease of the W cation size causes an increase of twisting, accompanied by axial elongation and radial compression. Metrically, *c* becomes longer, whereas *a* (and *b*) contract (Palmer et al. 1997). The twisting mechanism can also be observed in tetragonal analcime (cf. Fig. 6). The relative rotation of the

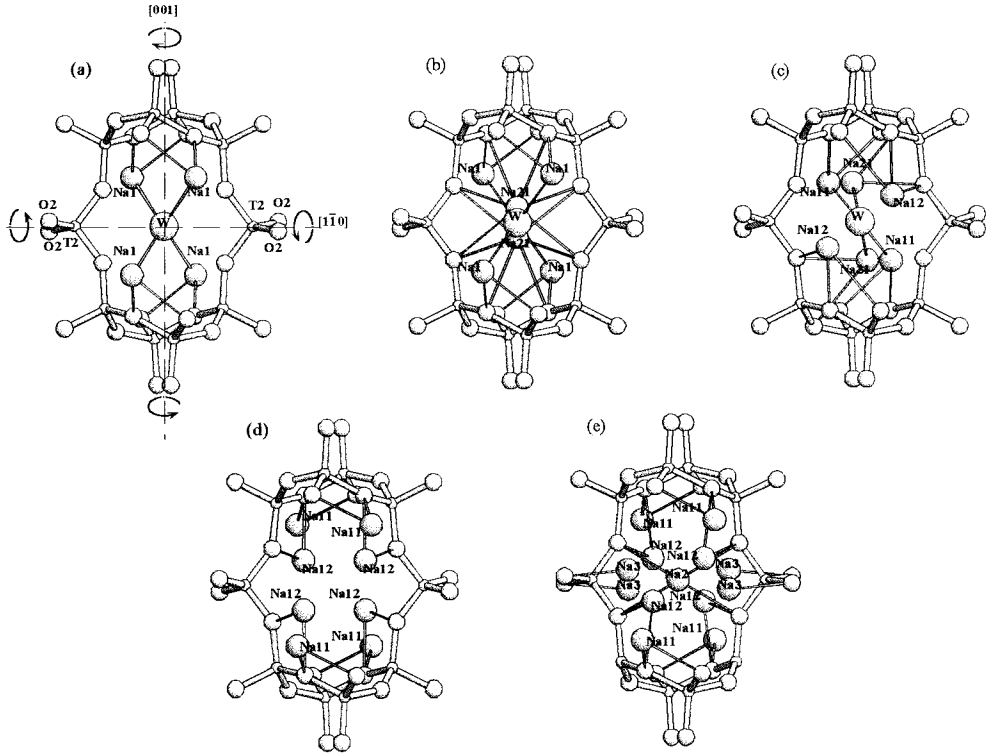

FIGURE 6. Stick and ball projections along [110], showing the eight-membered ring, as refined at (**a**) $T = 298$ K, (**b**) $T = 528$, (**c**) $T = 632$ K, (**d**) $T = 734$ K, and (**e**) $T = 921$ K. Pair-forbidden extraframework positions have been omitted for clarity. The twisting of the tetragonal prism around [001] and the associated counter-rotations of the T2 tetrahedra along [1$\bar{1}$0] are also depicted in **a**.

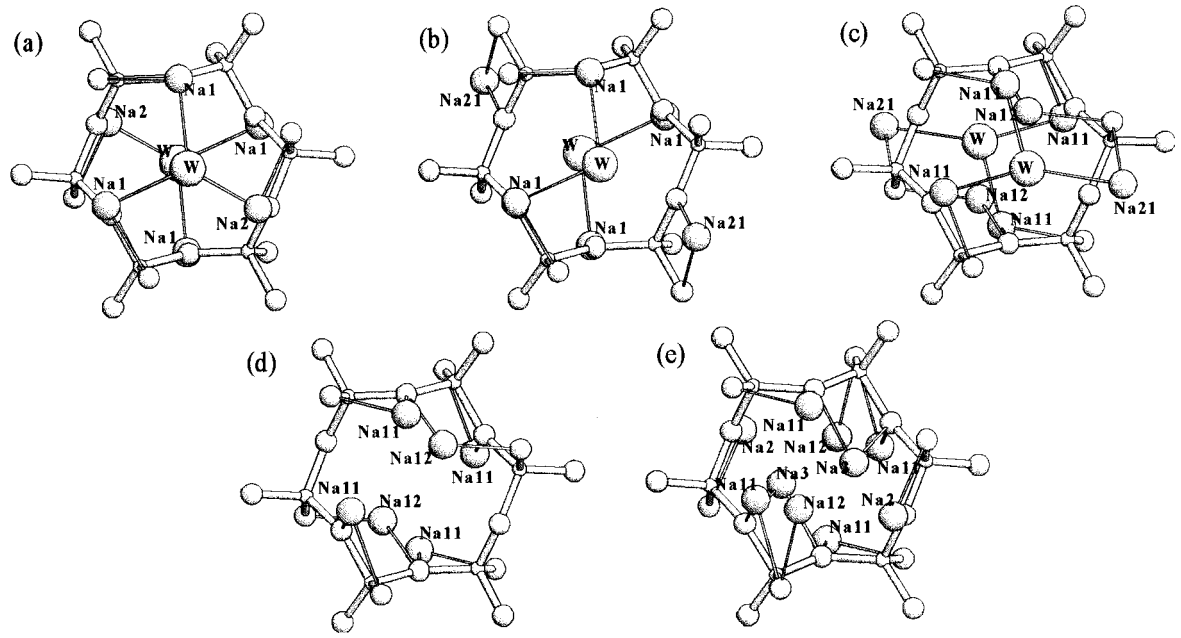

FIGURE 7. Stick and ball projections along [111], showing the six-membered ring, as refined at (**a**) T = 298 K, (**b**) T = 528, (**c**) T = 632 K, (**d**) T = 734 K, and (**e**) T = 921 K. Pair-forbidden extraframework positions have been omitted for clarity.

four-member rings of the tetragonal prism about [001] induces an opposite tilting of the T2 tetrahedra about [1$\bar{1}$0], as depicted in Figure 6a. This tilting angle can be used to monitor the twisting as a function of temperature. As a reference value, the tilting angle in cubic analcime (Ferraris et al. 1972) is about 5.4°. Figure 8 shows that the tilting of T2 about [1$\bar{1}$0] reaches a maximum at 650 K, then decreases again to a value close to the initial one. Comparing the behavior of T-O-T angles and tilting in Figure 8, it becomes clear that the opening of the six-member rings induced by the migration of H_2O molecules along [111] is accompanied by tilting of the T2 tetrahedra about [1$\bar{1}$0]. Furthermore, comparison of Figure 8 with Figure 3 shows that the temperature-dependent variations of the cell parameters and symmetry indicators are closely related to the distortion of the framework. In particular, the increased *a-c* difference up to 650 K is associated to the twisting increase, in agreement with the axial elongation and radial compression. Above 650 K the mechanism is inverted, and the *a-c* difference decreases consistently with the twisting decrease.

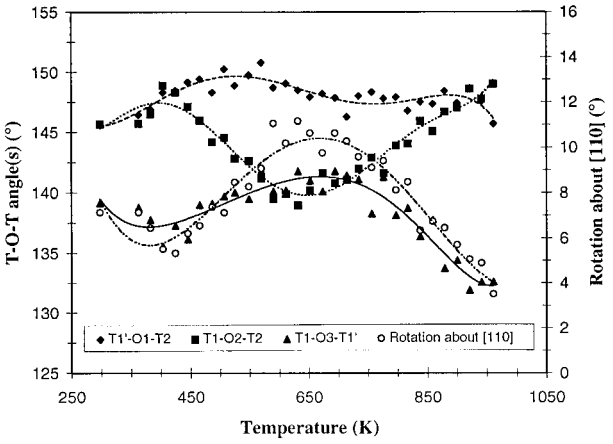

FIGURE 8. Variations of the T-O-T angles (see legend for symbols; left axis) and the rotation angle around [1$\bar{1}$0] (circles; right axis) vs. temperature ($T \pm 5$ K). The rotation angle is calculated as $\alpha = \sin^{-1}[c\ (3/4 - 2z_{O2})/d(\text{O2-O2})\ ]$, where d(O2-O2) = tetrahedral edge ≈ 2.716 Å. The curves are guides to the eye.

We may suggest that the above mechanism of tetrahedra tilting—accompanying the formation of wide-open six-member ring apertures along the [111] channels—is not energetically favored, because it would increase the elastic energy of the system. As a consequence, the water diffusion through the [111] channels requires H_2O molecules to have a substantial thermal energy. This behavior might be regarded as indirect evidence that the [111] channels represent a forced pathway for thermal activated water migration in the analcime structure.

The initial opening of wide six-member ring apertures induced by the diffusion of H_2O molecules through the channels during dehydration, combined with the consequent relaxation of the T-O-T angles back to the starting value, provides a key to understanding the ''anomalous'' negative thermal expansion (i.e., volume contraction during temperature increase) of dehydrated analcime. The same phenomenon in cubic analcime (Line 1995) has recently been discussed by Hammonds et al. (1996) on the grounds of the rigid-unit modes (RUM) theory (Dove

1997, and references therein). According to this model, the effect of any RUM distortion is to reduce the volume of the structure by an amount proportional to the average square of the rigid-unit rotation angles. Because this parameter is larger at higher temperatures, it leads to a greater volume reduction and hence a negative thermal expansion in dehydrated analcime (Hammonds et al. 1996). Our study of the thermal behavior of tetragonal analcime provides a complementary picture of the negative expansion phenomenon. The formation of wide-open six-member ring apertures along the sixfold channels during water migration is likely associated to a relative expansion of the framework. This relative expansion is not reflected in the cell volume variation (cf. Fig. 3), because the effect is overcompensated by the cell contraction related to the loss of water. After all the water is removed ($T > 650$ K), the restoration of the original T-O-T angles (cf. Fig. 8) leads to a further volume contraction. This contraction is more important than the volume increase due to thermal expansion of tetrahedra, which would be expected in the anhydrous phase, and as actually observed in leucite (Palmer et al. 1997). Unlike analcime, no formation of wide-open six-member rings occurs in the preceding stages of thermal treatment of leucite, which explains why the ''anomalous'' negative thermal expansion is not found in the latter case.

Acknowledgments

This work, carried out at Brookhaven National Laboratory (BNL), was supported under contract DE-AC02-76CH00016 with the U.S. Department of Energy by its Division of Chemical Sciences, Office of Basic and Energy Sciences. Financial support from ASI (supervisor G. Artioli, University of Milan), Italian CNR and MURST was also given to the authors. We are grateful to J.C. Hanson (Chemistry Department, BNL, U.S.A.) for his assistance during data collection at the X7B beamline (NSLS). Thanks are due to G. Artioli for the helpful discussion, to G. Vezzalini for performing the chemical analysis at the electron microprobe facility at the Dipartimento di Scienze della Terra, University of Modena, and to L. Bruce for the stylistic English improvement of the manuscript. We finally wish to thank A. Putnis (University of Cambridge, U.K.), W. Depmeier (University of Kiel, Germany), and R.T. Downs (University of Arizona, U.S.A.) whose critical reviews greatly improved the manuscript.

References cited

Calleri, M. and Ferraris, G. (1964) Struttura dellíanalcime: $NaAlSi_2O_6 \cdot H_2O$. Atti dell'Accademia delle Scienze di Torino, 98, 821–846.

Dove, M.T. (1997) Theory of displacive phase transitions in minerals. American Mineralogist, 82, 213–244.

Donovan, J.J. (1995) PROBE: PC-based data acquisition and processing for electron microprobes. Advanced Microbeam, 4217 C Kings Graves Rd., Vienna, Ohio, 44473.

Ferraris, G., Jones, D.W., and Yerkess, J. (1972) A neutron-diffraction study of the crystal structure of analcime, $NaAlSi_2O_6 \cdot H_2O$. Zeitschrift für Kristallographie, 135, 240–252.

Giampaolo, C. and Lombardi, G. (1994) The thermal behaviour of analcimes from two different genetic environments. European Journal of Mineralogy, 6, 285–289.

Gottardi, G. and Galli, E. (1985) Natural zeolites, 409 p. Springer-Verlag, Berlin.

Hammonds, K.D., Dove, M.T., Giddy, A.P., Heine, V., and Winkler, B. (1996) Rigid-unit phonon modes and structural phase transitions in framework silicates. American Mineralogist, 81, 1057–1079.

Hastings, J.B., Suortti, P., Thomlinson, W., Kvick, Å., and Koetzle, T.F. (1983) Optical design for the NSLS crystallographic beam line. Nuclear Instruments and Methods, 208, 55–58.

Hazen, R.M. and Finger, L.W. (1979) Polyhedral tilting: a common type of pure displacive phase transition and its relationship to analcite at high pressure. Phase Transitions, 1, 1–22.

Kapusta, J. and Wlodyka, R. (1997) The X-ray powder diffraction profile analysis of analcimes from the teschenitic sills of the Outer Carpathians, Poland. Neues Jahrbuch Für Mineralogie, Monatshefte, 6, 241–255.

Kim, K.T. and Burley, B.J. (1971) Phase equilibria in the system $NaAlSi_3O_8$–$NaAlSiO_4$–H_2O with special emphasis on the stability of analcite. Canadian Journal of Earth Sciences, 8, 311–338, 549–558, 558–572.

——(1980) A further study of analcime solid solutions in the system $NaAlSi_3O_8$–$NaAlSiO_4$–H_2O with particular note of an analcime phase transformation. Mineralogical Magazine, 43, 1035–145.

Knowles, C.R., Rinaldi, F.F., and Smith, J.V. (1965) Refinement of the crystal structure of analcime. Indian Mineralogist, 6, 127–140.

Larson, A.C. and Von Dreele, R.B. (1997) GSAS. General Structure Analysis System. Report LAUR 86-748, Los Alamos National Laboratory, Los Alamos, New Mexico.

Line, C.M.B. (1995) The behaviour of water in analcime. Ph.D. thesis, University of Cambridge, Cambridge, U.K.

Line, C.M.B., Putnis, A., Putnis, C., and Giampaolo, C. (1995) The dehydration kinetics and microtexture of analcime from two parageneses. American Mineralogist, 80, 268–279.

Line, C.M.B., Dove, M.T., Knight, K.S., and Winkler, B. (1996) The low-temperature behaviour of analcime. 1: High-resolution neutron powder diffraction. Mineralogical Magazine, 60, 499–507.

Luhar, J.F. and Kyser, T.K. (1989) Primary igneous analcime: the Colima minettes. American Mineralogist, 74, 216–223.

Mazzi, F. and Galli, E. (1978) Is each analcime different? American Mineralogist, 63, 448–460.

Merlino, S. (1984) Feldspathoids: Their average and real structure. In W.L. Brown, Ed., Feldspars and Feldspathoids, p. 435–470. Reidel, Dordrecht, the Netherlands.

Norby, P. (1997) Synchrotron powder diffraction using imaging plates: crystal structure determination and Rietveld refinement. Journal of Applied Crystallography, 30, 21–30.

Palmer, D.C., Dove, M.T., Ibberson, R.M., and Powell, B.M. (1997) Structural behavior, crystal chemistry, and phase transitions in substituted leucite: high-resolution neutron powder diffraction studies. American Mineralogist, 82, 16–29.

Putnis, A., Giampaolo, G., and Graeme-Barber, A. (1993) High temperature X-ray diffraction and thermogravimetric analysis of the dehydration of analcime, $NaAlSi_2O_6 \cdot H_2O$. EUG VII, Strasbourg 1993, Terra Abstracts, vol. 5, P497.

Taylor, W.H. (1930) The structure of analcite ($NaAlSi_2O_6 \cdot H_2O$). Zeitschrift für Kristallographie, 74, 1–19.

Manuscript received February 26, 1998
Manuscript accepted Steptember 3, 1998
Paper handled by Gilberto Artioli